

Constraining sub-GeV dark matter with Migdal and Boosted effects

Victor V. Flambaum,^{1,2,*} Liangliang Su,^{3,4,†} Lei Wu,^{3,‡} and Bin Zhu^{4,5,§}

¹*School of Physics, University of New South Wales, Sydney 2052, Australia*

²*Johannes Gutenberg-Universität Mainz, 55128 Mainz, Germany and Helmholtz-Institut, GSI Helmholtzzentrum für Schwerionenforschung, 55128 Mainz, Germany*

³*Department of Physics and Institute of Theoretical Physics, Nanjing Normal University, Nanjing, 210023, China*

⁴*School of Physics, Yantai University, Yantai 264005, China*

⁵*Department of Physics, Chung-Ang University, Seoul 06974, Korea*

(Dated: January 18, 2022)

Given the current strong constraints on WIMPs, search for sub-GeV Dark Matter (DM) now is an essential task in direct detections. In order to overcome the limitation of low recoils, enhancing ionization rate of electron from Migdal effect and modifying the velocity distribution of DM from interaction of DM and cosmic rays are two important ways. In this work, we find that these two ways are complementary to probe sub-GeV DM. The former can cover heavier DM, while the latter can cover the lighter DM. Both of them can cover DM with a mass of 20 MeV to 200 MeV. Including momentum transfer effect can greatly improve the existing bounds.

INTRODUCTION

The existence of dark matter (DM) has been supported by cosmological and astrophysical observations, however its properties, including its mass and interactions, are still elusive. As an attractive dark matter candidate, the Weakly Interacting Massive Particle (WIMP) [1] has been extensively studied in direct detection, indirect detection and collider experiments. With unprecedented sensitivity, the current direct detections that measure the nuclear recoils have produced very stringent limits on the WIMP dark matter. This motivates a broad investigation of light dark matter particles [2, 3].

However, the sub-GeV DM particles usually produce small energy deposited in an elastic nuclear recoil, $E_R \sim m_\chi^2 v_\chi^2 / m_N \sim 0.1$ eV, which is much below the threshold of traditional noble liquid detectors. Therefore, new technologies and detectors have been developed to search for sub-GeV scale DM particles, see e.g. [4–14].

Due to non-instantaneous movement of electron cloud during a nuclear recoil event, the recoil atom is either excited or ionized, and then immediately de-excites through the X-ray transition, the Auger transition, or the Coster-Kronig transition, which deposit additional energy inside the detector [15]. The first effect is so-called Migdal scattering [16] that can take place in a very low energy nuclear recoil, which has been used to extend the coverage of the low mass DM in noble liquid targets and semiconductors [8, 9, 17–25].

On the other hand, there are some astrophysical sources that can naturally boost the non-relativistic light dark matter by imparting the energy from the Standard Model particles to the dark matter. For examples, a small component of light dark matter in the halo can be elastically scattered by the high energy primary cosmic rays, and then obtains the sufficient kinetic energy to reach the sensitivity of traditional detectors [26–36]. Besides,

light dark matter can also come from light meson decays produced in the inelastic collision of cosmic rays with the atmosphere [37, 38]. By inheriting the parent velocity, such a light dark matter can move fast as well, and generate the detectable scintillation or ionization signal in direct detection. Also, light dark matter interacting with fast moving nuclei or electrons inside the Sun can be accelerated above threshold [39].

Since both of above two effects can enhance the sensitivity of searching for light DM, it is interesting to explore their complementarity of them in probing sub-GeV DM in direct detections. We will firstly compute the event rates of DM with Migdal and Boosted effects. In particular, we include the momentum transfer effect, which can enhance the scattering cross section as the momentum transfer is large enough. Then, with the Xenon1T data, we will calculate the exclusion limits and compare them with other existing result.

CALCULATION FRAMEWORK

We start from the calculations of Migdal scattering in the direct detection. The differential event rate of ionization electron with units per tonne per year per keV is given by,

$$\frac{dR_{ion}}{dE_e} = N_T \Phi_{halo} \sum_{nl} \frac{d\langle \sigma_{ion}^{nl} v \rangle}{dE_e}. \quad (1)$$

where $N_T = 4.2 \times 10^{27}$ is number density of Xenon per tonne and Φ_{halo} is the flux of halo DM. The velocity-averaged ionization cross section $\langle \sigma_{ion}^{nl} v \rangle$ can be written as [8]

$$\begin{aligned} \frac{d\langle \sigma_{ion}^{nl} v \rangle}{dE_e} &= \frac{[f_p Z + f_n (A - Z)]^2}{8\mu_n^2 E_e} \int_{q_{min}} dq q \\ &\times \sigma_n |F_N(q)|^2 |f_{nl}^{ion}(p_e, q_e)|^2 \eta(E_{X,min}), \end{aligned} \quad (2)$$

where Z is the atomic number and A is the mass number of atom. $f_{p,n}$ are dimensionless couplings of DM with proton and neutron and are taken as $f_p = f_n$ in our scenario due to isospin conservation. $\mu_{\mathbf{n}} = m_{\chi} m_{\mathbf{n}} / (m_{\chi} + m_{\mathbf{n}})$ is the DM and nucleon reduced mass. E_e and p_e are the energy and momentum of ionized electron, respectively. q and q_e are the transfer momenta of nucleus and electron. The value of q_{min} should be able to ionize the electrons in the first shell, while the maximal value of q is determined by kinetic energy of incoming DM, T_{χ}^{\max} .

In Eq. 2, the DM-nucleon scattering cross section $\sigma_{\mathbf{n}}$ can be written as,

$$\sigma_{\mathbf{n}} = \bar{\sigma}_{\mathbf{n}} |F_{\text{DM}}(q)|^2 \quad (3)$$

where the momentum independent cross section $\bar{\sigma}_{\mathbf{n}}$ is defined by

$$\bar{\sigma}_{\mathbf{n}} \equiv \mu_{\mathbf{n}}^2 \frac{|\mathcal{M}_{\mathbf{n}}(q=q_0)|^2}{(16\pi m_{\chi}^2 m_{\mathbf{n}}^2)}. \quad (4)$$

and the momentum-dependent factor $F_{\text{DM}}(q)$ is given by,

$$|F_{\text{DM}}(q)|^2 \equiv \frac{|\mathcal{M}_{\mathbf{n}}(q)|^2}{|\mathcal{M}_{\mathbf{n}}(q=q_0)|^2} \quad (5)$$

where the reference momentum $q_0 = \alpha m_e$. It should be noted that the exact forms of $\sigma_{\mathbf{n}}$ and F_{DM} are model-dependent. For the contact interaction, $F_{\text{DM}}(q) = 1$. While including the light mediator effect, $F_{\text{DM}}(q)$ will rely on the momentum transfer, which will be given in next section.

For xenon, we use the Helm form factor for the nucleus form factor $F_N(q)$, which is given by [40],

$$|F_N|^2 = \left(\frac{3j_1(qR_1)}{qR_1} \right)^2 e^{-q^2 s^2} \quad (6)$$

with

$$j_1(x) = \frac{\sin x}{x^2} - \frac{\cos x}{x} \quad (7)$$

being a spherical Bessel function of the first kind. R_1 and s are the effective nuclear radius and skin thickness, respectively. Their values for the Helm form factor that can reproduce the numerical fourier transform of a Two-Parameter Fermi distribution are taken as

$$R_1(x) = \sqrt{c^2 + \frac{7}{3}\pi^2 a^2 - 5s^2}, \quad s = 0.9 \text{ fm} \quad (8)$$

where $a = 0.52 \text{ fm}$ and $c = (1.23A^{1/3} - 0.60) \text{ fm}$.

Since we are considering the (non-)relativistic DM, the velocity distribution η has to be generalized to include the contributions from fast-moving DM,

$$\eta(E_{\chi, \min}) = \int_{E_{\chi, \min}} dE_{\chi} \Phi_{\text{halo}}^{-1} \frac{m_{\chi}^2}{p_{\chi} E_{\chi}} \frac{d\Phi_{\chi}}{dE_{\chi}} \quad (9)$$

where $E_{\chi} = m_{\chi} + T_{\chi}$ and $d\Phi_{\chi}/dE_{\chi}$ is the differential flux of DM, which depends on the acceleration mechanism of DM (see details in following section). For the non-relativistic DM, such as standard DM in halo, η will become the Maxwell-Boltzmann velocity distribution.

The lower limit of integration of DM incoming energy $E_{\min, \chi}$ can be obtained from DM-atom scattering process $\chi(p) + A(k) \rightarrow \chi(p') + A(k')$. With energy conservation, we can have the minimal value of DM momentum, $E_{\chi, \min} = (q + E_{\text{EM}})/2$ in the limit of massless DM, where $E_{\text{EM}} = E_{nl} + \Delta E_e$.

Next, we discuss ionization factor $|f_{nl}^{\text{ion}}(p_e, q_e)|^2$ in Eq. 2. It is proportional to the possibility that electrons in an atom are ionized during a nuclear recoil in inelastic collisions between dark matter and atom [17]. For simplicity, we will not include the secondary contributions from de-excitation electron and X-rays in this work. We assume that $|i\rangle$ and $|i'\rangle$ are the states of electron cloud of atom before and after a nuclear recoil, respectively. The transition matrix of the state $|i'\rangle$ to the ionization/excitation state $|f\rangle$ of atom can be given by, $\langle f | i' \rangle_M = \langle f | e^{-i \frac{m_e}{m_A} \vec{q} \cdot \sum_s \vec{x}^s} | i \rangle \approx \langle f | e^{-i \frac{m_e}{m_N} \vec{q} \cdot \sum_s \vec{x}^s} | i \rangle$, where m_e , m_A and m_N are the masses of electron, atom and nucleus, respectively. \vec{x}^s denotes the position of s^{th} electron in electron cloud. $\vec{q}(\vec{v})$ is three momentum transfer in the DM-atom scattering process. Different from DM-electron scattering, the total momentum transfer in Migdal scattering is partly impeded to the electron, $q_e \simeq m_e/m_N q$. Although there is a suppression factor $m_e/m_N \sim 10^{-6}$ for Xenon, the energy loss as heat is negligible due to the small mass of electron.

It should be noted that the ionization factor can be approximately evaluated by using the plane wave with the Sommerfeld enhancement factor. However, we find that such an approximation works well for large q . When q becomes small, the result will strongly depend on the choice of reference transfer momentum q_0 , and can have a sizable deviation from those non-relativistic solutions in [10, 41] because out-going electron is affected by effective potential rather than a free electron. In our study, we compute the ionization factor by numerically solving Schrodinger equation with a certain potential. We include the contributions from electron configurations of $4s$, $4p$, $4d$, $5s$ and $5p$. We also compare the result with that from the package DarkARC [41] and found that they are consistent within the accuracy. Besides, since the momentum transfer to electron in Migdal scattering is small, we will not include the relativistic correction to ionization factor f_{nl}^{ion} [42].

Then, we can use the differential ionization rate dR_{ion}/dE_e in Eq. 1 and S2 data of the Xenon1T to derive the exclusion limit by

$$\frac{dR_{ion}}{dS2} = \int dE_e \epsilon(S2) P(S2 | E_{\text{EM}}) dR_{ion}/dE_e \quad (10)$$

where $\epsilon(S2)$ is the detector efficiency. The probability

function P that converts energy transfer into the photoelectron (PE) in S2 is given by

$$P(S2 | E_{EM}) = \sum_{n_e^s, n_e} P(S2 | n_e^s) \cdot P(n_e^s | n_e) \cdot P(n_e | \langle n_e \rangle) \quad (11)$$

Here $P(n_e | \langle n_e \rangle) = C_{N_Q}^{n_e} f_e^{n_e} (1 - f_e)^{N_Q - n_e}$ is the number of electrons escaping the interaction point, where $N_Q = E_{EM}/(13.8 \text{ eV})$ and $f_e = \langle n_e \rangle / N_Q \sim 0.83$. The possibility of electrons surviving the drift in Xenon1T is taken as $P(n_e^s | n_e) = 80\%$. Finally the survival electrons have to be converted into PE in S2 with the possibility $P(S2 | n_e^s) = \text{gauss}(S2 | g_2 n_e^s, \sigma_{S2})$, where $\sigma_{S2} = 7\sqrt{n_e^s}$ and $g_2 = 33$ for Xenon1T.

As for the fast-moving DM, it should be mentioned that the conventional nucleus recoil data of DM-nucleus scattering may also provide strong bounds due to the DM having enough kinetic energy DM. In order to obtain the corresponding limits, we need to replace the E_e with E_R and take $|f_{nl}^{\text{ion}}|^2 = 1$ in Eq. 2 to compute the differential rate of DM-nucleus scattering process.

BENCHMARK MODEL

In order to perform our numerical calculation, we will study a simplified hadrophilic DM model, where a flavor-specific singlet scalar mediator S couples to up-type quarks and DM [43]. The effective interactions can be written as follows,

$$\mathcal{L} = i\bar{\chi} (\not{D} - m_\chi) \chi + \frac{1}{2} \partial_\mu S \partial^\mu S - \frac{1}{2} m_S^2 S^2 - (g_\chi S \bar{\chi}_L \chi_R + g_u S \bar{u}_L u_R + \text{h.c.}) \quad (12)$$

where m_S and m_χ are the masses of mediator and DM, respectively. g_χ and g_u are the couplings of mediator S with the DM and up-quarks, respectively. With Eq. 12, we can obtain the momentum independent DM-nucleon scattering cross section $\bar{\sigma}_n$ in Eq. 4,

$$\bar{\sigma}_n \equiv \mu_n^2 \frac{|\mathcal{M}_n(q=q_0)|^2}{(16\pi m_\chi^2 m_N^2)} = \frac{g_n^2 g_\chi^2 \mu_n^2}{\pi (\alpha^2 m_e^2 + m_s^2)^2}, \quad (13)$$

where $q_0 = \alpha m_e$ and $g_n = 0.014 g_u (m_p/m_u)$. The DM momentum-dependent factor F_{DM} in Eq. 5 can be written as,

$$|F_{DM}(q)|^2 = \frac{(4m_n^2 + q^2) (m_s^2 + q_0^2)^2 (4m_\chi^2 + q^2)}{16m_n^2 m_\chi^2 (m_s^2 + q^2)^2}. \quad (14)$$

As an example of fast-moving DM, we investigate the atmospheric DM, which is produced in the inelastic collision of high energy CRs with the atmosphere on Earth [37, 38]. For simplicity, we only include the contribution of proton in the CRs and parameterize it as

Ref. [44]. We focus on the production process of ADM,

$$p + N \rightarrow M \rightarrow \chi\bar{\chi} + X \quad (15)$$

where p is proton and N is nitrogen. The light meson M produced in collision is taken as η for example, which will decay to a pair of DM $\chi\bar{\chi}$ via an on-shell scalar mediator ¹. X denotes other SM particle.

The differential flux of ADM is given by,

$$\frac{d\phi_\chi}{dT_\chi} = G \int_{T_p^{\min}}^{T_p^{\max}} \frac{dT_p}{\Omega(T_p)} \frac{d\phi_p(h_{\max})}{dT_p} \frac{d\sigma_{pN \rightarrow \chi\bar{\chi}X}}{dT_\chi} \quad (16)$$

where the CRs differential flux $d\phi_p/dT_p = y_p(h) \frac{d\phi_p(T_p, h_{\max})}{dT_p}$, and inelastic differential cross section $d\sigma_{pN \rightarrow \pi\chi\bar{\chi}}/dT_\chi \simeq \frac{\sigma_{pN}}{T_\chi^{\max}} \text{BR}(M \rightarrow \chi\bar{\chi}X) T_p$ is the proton energy and h is the height from the ground level.

The geometrical factor G of ADM can be calculated by

$$G = 2\pi \int_0^{h_{\max}} dh \int_{-1}^{+1} d\cos\theta (R_E + h)^2 \frac{y_d y_p}{\ell_d^2} n_N(h) \quad (17)$$

where n_N is the number density of nitrogen. l_d is the line of sight distance between the production point of DM and the detector, $\ell_d^2 = (R_E + h)^2 + (R_E - h_d)^2 - 2(R_E + h)(R_E - h_d)\cos\theta$ where $h_d = 1.4 \text{ km}$ is the depth of the detector, and θ is the polar angle of the DM production point. The dilution factor of incoming CRs in atmosphere y_p and attenuation factor of DM in the Earth y_d are given by $y_p = \exp\left(-\sigma_{pN} \int_h^{h_{\max}} d\tilde{h} n_N(\tilde{h})\right)$ and $y_d = \exp\left(-\sigma_{\chi N} \int_0^{l_d} dz n(r(z) - R_E)\right)$ respectively, where $h_{\max} = 180 \text{ km}$ and $R_E = 6378.1 \text{ km}$. n is the number density of nucleus at the depth of $r(z) - R_E$. σ_{pN} and $\sigma_{\chi N}$ are the proton-nitrogen and DM-nucleus scattering cross section, respectively. We use the package CRMC [45–47] to simulate the above inelastic collision of incoming CRs with the nitrogen.

Since our ADMs are produced via the decay of on-shell mediator S , we will investigate the mass range of $m_S < m_\eta - m_\pi$. When $m_S < m_\pi$, the coupling g_u is tightly constrained by the null result of $K \rightarrow \pi\nu\bar{\nu}$ in E787/949 experiment [48–51], which requires $g_u \lesssim 4 \times 10^{-6}$. If $m_S < 2m_\pi$, the decay of S to diphotons will increase the deuterium abundance $D/H = (2.53 \pm 0.04) \times 10^{-5}$ and further affect the baryon-to-photon ratio. In terms of existing bounds, we find the bound $m_S > 20 \text{ MeV}$ and $g_u > (2 \times 10^{-8}) \left(\frac{m_S}{\text{GeV}}\right)^{-3/2}$. On the other hand, when $m_\pi < m_S < m_K - m_\pi$, MINIBOONE experiment [52]

¹ In principle, neutral π can also be the source of ADM. However, the current limit on $Br(\pi \rightarrow \gamma + \text{invisible}) < 10^{-9}$ make its contribution to the ADM flux negligible. On the other hand, the decays of other charged mesons are more model-dependent. We will not include them in our calculations.

gives an upper bound $g_u \lesssim 4 \times 10^{-5}$. This is stronger than the bound derived from the Xenon1T data. Therefore, in order to escape these constraints, we take $g_u = 10^{-5}$ and $m_S = 300$ MeV as our benchmark point, which corresponds to $Br(\eta \rightarrow \pi\chi\bar{\chi}) \simeq 1 \times 10^{-5}$.

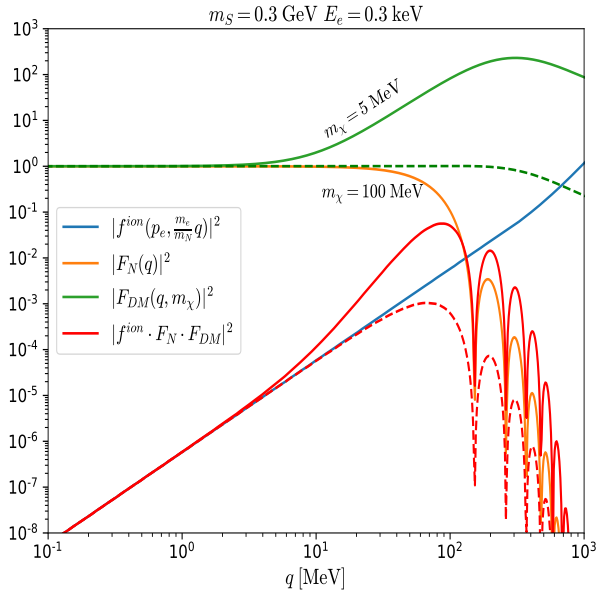


Figure 1. The dependence of ionization factor $|f_{nl}^{ion}(p_e, q_e)|^2$, nucleus form factor $|F_N(q)|^2$ and DM momentum-dependent factor $|F_{DM}(q)|^2$ on the nucleus momentum transfer q . Two benchmark points $m_\chi = 5$ MeV (solid line) and $m_\chi = 100$ MeV (dashed line) are shown.

NUMERICAL RESULTS AND DISCUSSIONS

In Fig. 1, we show the dependence of ionization factor, nucleus form factor and DM momentum-dependent factor on nucleus momentum transfer q at $E_e = 0.3$ keV and $m_S = 0.3$ GeV. We can see that the $|f_{nl}^{ion}(p_e, q_e)|^2$ is enhanced by about eight orders when q is varied from about 0.1 MeV to 1 GeV. The DM momentum-dependent factor $|F_{DM}(q)|^2$ depends on the mass of DM. For lighter DM, such as $m_\chi = 5$ MeV, $|F_{DM}(q)|^2$ can reach about $\mathcal{O}(10^2)$, while for heavier DM, $|F_{DM}(q)|^2$ will be less than one. But in the range of $q \gtrsim 300$ MeV, they will decrease rapidly. Besides, we can find that the nucleus form factor $|F_N|^2$ is highly suppressed in the range of $q \gtrsim 100$ MeV.

In Fig. 2, we compare the differential event rates of DM-nucleus scattering process in the cases of ADM (relativistic DM) and Migdal effect (non-relativistic DM). We can see that the differential rate of ADM is small but its boosted recoil E_R can be about $\mathcal{O}(\text{MeV})$ because of the boosted effect of the meson decay. This can make the light ADM reach the threshold of nucleus recoil signal ($E_R \sim 1$ keV) in Xenon experiments. Since the larger

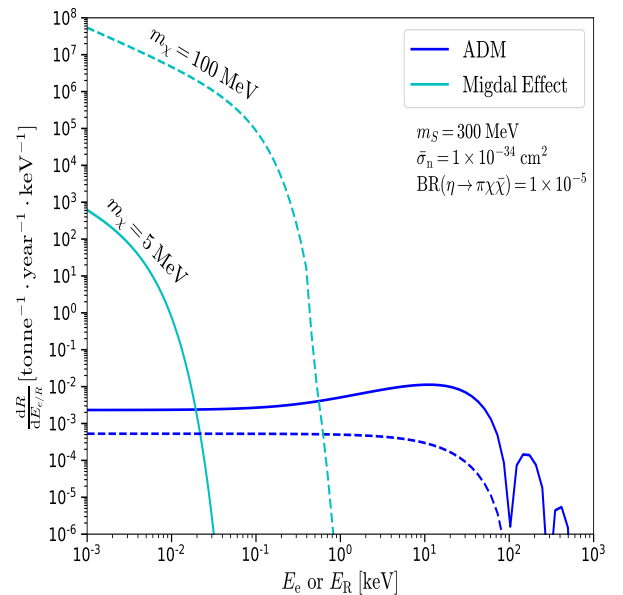


Figure 2. Differential event rates of DM-nucleus scattering process in the cases of ADM (relativistic DM) and Migdal effect (non-relativistic DM), where E_R is the nucleus recoil and E_e is the energy of ionization electron. The solid and dashed lines correspond to DM mass $m_\chi = 5$ MeV and 100 MeV, respectively. We assume the mediator mass $m_S = 300$ MeV, the branching ratio $Br(\eta \rightarrow \pi\chi\bar{\chi}) = 10^{-5}$ and momentum-independent DM-nucleon scattering cross section $\bar{\sigma}_n = 10^{-34}$ cm^2 .

flux of CRs lies in the low energy range, the lighter DM has a larger differential rate than the heavier DM. On the other hand, it can be seen that the Migdal scattering has sizable events in the low ionization electron energy E_e . We also checked the Migdal effect in ADM, we found that the event rate of such a scenario is much smaller than that of the Migdal scattering. This is because that the DM in this case has a high velocity and can produce a larger momentum transfer, which will lead to the suppression of the nucleus form factor F_N .

In Fig. 3, we use the Xenon1T ionization [53] and nucleus recoil data to derive the exclusion limits on the momentum-independent DM-nucleon scattering cross section $\bar{\sigma}_n$ for above cases. As a comparison with the result in Ref. [37], we present their limit by scaling the branching ratio $Br(\eta \rightarrow \pi\chi\bar{\chi})$ from 10^{-3} to 10^{-5} as well. We can see that the Migdal scattering can exclude the DM mass down to about 20 MeV, while the ADM can further exclude lower DM mass. The momentum-independent non-relativistic DM-nucleon with Migdal and relativistic DM-nucleon scattering cross section can be excluded down to about 10^{-37} cm^2 at $m_\chi = 0.2$ GeV and 10^{-35} cm^2 at $m_\chi = 0.1$ MeV, respectively. They are complementary in probing sub-GeV DM. Besides, when $m_\chi \lesssim 100$ MeV, it should be noted that the enhancement effect of DM momentum-dependent factor in Eq. 14

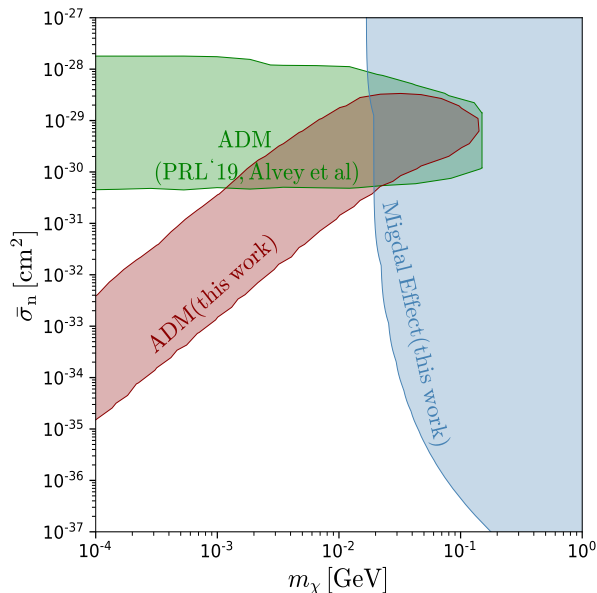


Figure 3. Exclusion limits on the momentum-independent DM-nucleon scattering cross section $\bar{\sigma}_n$ in the cases of ADM with $F_{\text{DM}} = 1$ (green shaded region), ADM with F_{DM} in Eq. 14 (red shaded region) and Migdal scattering of non-relativistic DM (blue shaded region).

will be sizable and has to be taken into account, which leads to a much stronger limit than that in Ref. [37]. On the other hand, we also checked and find that the bound of ADM with Migdal effect is weaker than that of ADM because of the suppression of ionization factor. In other words, once the light DM can obtain enough kinetic energy, the current nucleus recoil data can provide a stronger limit than the ionization data. Besides, since the above results mainly depend on the velocity of DM, we can expect that other fast-moving DMs, such as cosmic ray up-scattering DM [27], will have similar conclusions.

Finally, we discuss the relic density of ADM in our interest of mass range, i.e. $m_\chi < m_S$, in which χ will annihilate directly to the SM quarks via a s-channel mediator. The cross section of annihilation is given by

$$\sigma v_{\text{rel}}(\chi\bar{\chi} \rightarrow q\bar{q}) = \frac{g_\chi^2 m_\chi v_{\text{rel}}^2 \Gamma_S|_{m_S=2m_\chi}}{2 \left((m_S^2 - 4m_\chi^2)^2 + m_S^2 \Gamma_S^2 \right)}, \quad (18)$$

which is suppressed by velocity. $\Gamma_S|_{m_S=2m_\chi}$ is the decay width of the scalar at $m_S = 2m_\chi$. The freeze-out scenario is guaranteed that $\Gamma_S > H[m_S]$, which in turn favors relatively larger coupling g_u . Thus DM is in chemical equilibrium with the early universe bath as long as it contains quarks. After the QCD phase transition takes place, DM pairs could still annihilate into two pions. Therefore achieving the correct relic density via thermal freeze-out would require $m_\chi > m_\pi$. For lighter DM, we

can allow for a small coupling of the mediator to neutrinos to achieve the correct relic abundance via thermal freeze-out [54].

Added Note : We have to point out that there is a conflict between the data in two Xenon1T papers [53] and [55]. The latter results (Figs. 2 and 4) will lead to two order enhancement of our exclusion limit in Migdal case.

ACKNOWLEDGMENTS

This work is supported by the National Natural Science Foundation of China (NNSFC) under grant No. 11805161, by Jiangsu Specially Appointed Professor Program, by Natural Science Foundation of Shandong Province under the grants ZR2018QA007 and by the Australian Research Council Grants No. DP190100974 and DP200100150. BZ is also supported by the Basic Science Research Program through the National Research Foundation of Korea (NRF) funded by the Ministry of Education, Science and Technology (NRF-2019R1A2C2003738), and by the Korea Research Fellowship Program through the NRF funded by the Ministry of Science and ICT (2019H1D3A1A01070937). We are grateful to Ben Roberts for a useful discussion.

* v.flambaum@unsw.edu.au

† liangliangsu@njnu.edu.cn

‡ leiwu@njnu.edu.cn

§ zhubin@mail.nankai.edu.cn

- [1] B. W. Lee and S. Weinberg, Phys. Rev. Lett. **39**, 165 (1977).
- [2] G. Bertone and M. Tait, Tim, Nature **562**, 51 (2018), 1810.01668.
- [3] S. Knapen, T. Lin, and K. M. Zurek, Phys. Rev. D **96**, 115021 (2017), 1709.07882.
- [4] Y. Hochberg, Y. Zhao, and K. M. Zurek, Phys. Rev. Lett. **116**, 011301 (2016), 1504.07237.
- [5] R. Essig, M. Fernandez-Serra, J. Mardon, A. Soto, T. Volansky, and T.-T. Yu, JHEP **05**, 046 (2016), 1509.01598.
- [6] K. Schutz and K. M. Zurek, Phys. Rev. Lett. **117**, 121302 (2016), 1604.08206.
- [7] G. F. Giudice, D. Kim, J.-C. Park, and S. Shin, Phys. Lett. B **780**, 543 (2018), 1712.07126.
- [8] M. Ibe, W. Nakano, Y. Shoji, and K. Suzuki, JHEP **03**, 194 (2018), 1707.07258.
- [9] M. J. Dolan, F. Kahlhoefer, and C. McCabe, Phys. Rev. Lett. **121**, 101801 (2018), 1711.09906.
- [10] R. Essig, T. Volansky, and T.-T. Yu, Phys. Rev. D **96**, 043017 (2017), 1703.00910.
- [11] J. Smirnov and J. F. Beacom (2020), 2002.04038.
- [12] J. A. Dror, G. Elor, R. McGehee, and T.-T. Yu (2020), 2011.01940.
- [13] J. Kozaczuk and T. Lin, Phys. Rev. D **101**, 123012 (2020), 2003.12077.

- [14] I. M. Bloch, A. Caputo, R. Essig, D. Redigolo, M. Sholapurkar, and T. Volansky (2020), 2006.14521.
- [15] K. D. Nakamura, K. Miuchi, S. Kazama, Y. Shoji, M. Ibe, and W. Nakano (2020), 2009.05939.
- [16] A. Migdal, *Sov.Phys.JETP* **9**, 1163 (1939).
- [17] R. Essig, J. Pradler, M. Sholapurkar, and T.-T. Yu, *Phys. Rev. Lett.* **124**, 021801 (2020), 1908.10881.
- [18] N. F. Bell, J. B. Dent, J. L. Newstead, S. Sabharwal, and T. J. Weiler, *Phys. Rev. D* **101**, 015012 (2020), 1905.00046.
- [19] D. Baxter, Y. Kahn, and G. Krnjaic, *Phys. Rev. D* **101**, 076014 (2020), 1908.00012.
- [20] C.-P. Liu, C.-P. Wu, H.-C. Chi, and J.-W. Chen (2020), 2007.10965.
- [21] Z.-L. Liang, C. Mo, F. Zheng, and P. Zhang (2020), 2011.13352.
- [22] Z.-L. Liang, L. Zhang, F. Zheng, and P. Zhang, *Phys. Rev. D* **102**, 043007 (2020), 1912.13484.
- [23] G. Grilli di Cortona, A. Messina, and S. Piacentini, *JHEP* **11**, 034 (2020), 2006.02453.
- [24] U. K. Dey, T. N. Maity, and T. S. Ray, *Phys. Lett. B* **811**, 135900 (2020), 2006.12529.
- [25] S. Knapen, J. Kozaczuk, and T. Lin (2020), 2011.09496.
- [26] C. V. Cappiello, K. C. Ng, and J. F. Beacom, *Phys. Rev. D* **99**, 063004 (2019), 1810.07705.
- [27] T. Bringmann and M. Pospelov, *Phys. Rev. Lett.* **122**, 171801 (2019), 1810.10543.
- [28] J. B. Dent, B. Dutta, J. L. Newstead, and I. M. Shoemaker, *Phys. Rev. D* **101**, 116007 (2020), 1907.03782.
- [29] K. Bondarenko, A. Boyarsky, T. Bringmann, M. Hufnagel, K. Schmidt-Hoberg, and A. Sokolenko, *JHEP* **03**, 118 (2020), 1909.08632.
- [30] W. Wang, L. Wu, J. M. Yang, H. Zhou, and B. Zhu (2019), 1912.09904.
- [31] G. Guo, Y.-L. S. Tsai, and M.-R. Wu, *JCAP* **10**, 049 (2020), 2004.03161.
- [32] S.-F. Ge, J.-L. Liu, Q. Yuan, and N. Zhou (2020), 2005.09480.
- [33] C. Xia, Y.-H. Xu, and Y.-F. Zhou (2020), 2009.00353.
- [34] G. Guo, Y.-L. S. Tsai, M.-R. Wu, and Q. Yuan, *Phys. Rev. D* **102**, 103004 (2020), 2008.12137.
- [35] J. Jaeckel and W. Yin (2020), 2007.15006.
- [36] Q.-H. Cao, R. Ding, and Q.-F. Xiang (2020), 2006.12767.
- [37] J. Alvey, M. Campos, M. Fairbairn, and T. You, *Phys. Rev. Lett.* **123**, 261802 (2019), 1905.05776.
- [38] L. Su, W. Wang, L. Wu, J. M. Yang, and B. Zhu (2020), 2006.11837.
- [39] H. An, M. Pospelov, J. Pradler, and A. Ritz, *Phys. Rev. Lett.* **120**, 141801 (2018), [Erratum: *Phys.Rev.Lett.* **121**, 259903 (2018)], 1708.03642.
- [40] G. Duda, A. Kemper, and P. Gondolo, *JCAP* **04**, 012 (2007), hep-ph/0608035.
- [41] R. Catena, T. Emken, N. A. Spaldin, and W. Tarantino, *Phys. Rev. Res.* **2**, 033195 (2020), 1912.08204.
- [42] B. Roberts, V. Dzuba, V. Flambaum, M. Pospelov, and Y. Stadnik, *Phys. Rev. D* **93**, 115037 (2016), 1604.04559.
- [43] B. Batell, A. Freitas, A. Ismail, and D. Mckeen, *Phys. Rev. D* **100**, 095020 (2019), 1812.05103.
- [44] M. Boschini et al., *Astrophys. J.* **840**, 115 (2017), 1704.06337.
- [45] T. Pierog, I. Karpenko, J. Katzy, E. Yatsenko, and K. Werner, *Phys. Rev. C* **92**, 034906 (2015), 1306.0121.
- [46] C. Baus, T. Pierog, and U. R., *Cosmic Ray Monte Carlo (CRMC)* (2019).
- [47] J. Alvey, <https://github.com/james-alvey-42/BoostedDM> (2019).
- [48] S. Adler et al. (E787), *Phys. Lett. B* **537**, 211 (2002), hep-ex/0201037.
- [49] S. Adler et al. (E787), *Phys. Rev. D* **70**, 037102 (2004), hep-ex/0403034.
- [50] S. Adler et al. (E949, E787), *Phys. Rev. D* **77**, 052003 (2008), 0709.1000.
- [51] A. Artamonov et al. (BNL-E949), *Phys. Rev. D* **79**, 092004 (2009), 0903.0030.
- [52] A. Aguilar-Arevalo et al. (MiniBooNE DM), *Phys. Rev. D* **98**, 112004 (2018), 1807.06137.
- [53] E. Aprile et al. (XENON), *Phys. Rev. Lett.* **123**, 251801 (2019), 1907.11485.
- [54] A. Berlin and N. Blinov, *Phys. Rev. Lett.* **120**, 021801 (2018), 1706.07046.
- [55] E. Aprile et al. (XENON), *Phys. Rev. Lett.* **123**, 241803 (2019), 1907.12771.